PCCP

Accepted Manuscript

ROYAL SOCIETY OF CHEMISTRY

www.rsc.org/pccp

Cite this: DOI:

www.rsc.org/xxxxxx

PAPER

Bringing light into the dark triplet space of molecular systems†

Jing Ge,[a] Qun Zhang,*[a,b,c] Jun Jiang,*[a,b,c] Zhigang Geng,[b] Shenlong Jiang,[b] Kaili Fan,[a] Zhenkun Guo,[a] Jiahua Hu,[a] Zongwei Chen,[a] Yang Chen,[a,b,c] Xiaoping Wang[b,c] and Yi Luo*[a,b,c,d]

Received (in XXX, XXX) Xth XXXXXXXXX 2015, Accepted Xth XXXXXXXXX 20XX

DOI:

A molecule or molecular system always consists of excited states of different spin multiplicities. With conventional optical excitations, only the (bright) states with the same spin multiplicity of the ground state could be directly reached. How to reveal the dynamics of excited (dark) states remains the grand challenge in the topical fields of photochemistry, photophysics, and photobiology. For a singlet–triplet coupled molecular system, the (bright) singlet dynamics can be routinely examined by conventional femtosecond pump–probe spectroscopy. However, owing to the involvement of intrinsically fast decay channels such as intramolecular vibrational redistribution and internal conversion, it is very difficult, if not impossible, to single out the (dark) triplet dynamics. Herein, we develop a novel strategy that uses an ultrafast broadband white-light continuum as the excitation light source to enhance the probability of intersystem crossing, thus facilitating the population flow from the singlet space to the triplet space. With a set of femtosecond time-reversed pump–probe experiments, we report on a proof-of-concept molecular system (i.e., the malachite green molecule) that the pure triplet dynamics can be mapped out in real time through monitoring the modulated emission that occurs solely in the triplet space. Significant differences in excited-state dynamics between the singlet and triplet spaces have been observed. This newly developed approach may provide a useful tool for examining the elusive dark-state dynamics of molecular systems and also for exploring the mechanisms underlying molecular luminescence/photonics and solar light harvesting.

Introduction

In recent years, the importance of the optically unreachable "dark" states, such as the triplet states in singlet–triplet coupled molecular systems, has been increasingly evident in many emerging photochemical and photophysical applications including photocatalysis,[1,2] organic light-emitting diodes,[3–6] and photovoltaics,[7,8] in which enhanced spin–orbit coupling or intersystem crossing (ISC) usually leads to greatly improved performance. In this context, detailed insights into the excited-state dynamics involved in singlet–triplet coupled molecular systems, in particular the role of the triplets, are highly desirable. However, it remains a grand challenge to glean information of spectral signatures as well as population dynamics in the dark triplet space.[9] Time-resolved photoluminescence spectroscopy is normally applicable only for monitoring the first excited singlet S_1 (fluorescence) or triplet T_1 (phosphorescence) due to the restriction of Kasha's rule.[10,11] The conventional femtosecond (fs) pump–probe measurements[12] often yield a picture of mixed-up singlet and triplet dynamics in which the transient signals are overwhelmed by contributions from the strongly allowed transitions in the bright singlet space, including ground-state bleach, stimulated emission, and excited-state absorption.[13] It is thus very difficult to single out and further map out the real-time excited-state dynamics evolving solely in the dark triplet space of molecular systems.

Herein, we introduce a strategy to overcome this difficulty with two basic ideas in mind. The first is to increase the ISC probability by applying an ultrafast broadband white-light continuum (WLC) as the excitation light source to populate vibrational manifolds in a certain excited singlet state. As the ISC efficiency can be enhanced by certain excited vibrational modes,[14,15] the use of broadband WLC that facilitates the excitation of different vibrational modes is expected to favor ISC and hence enhance population transfer from the excited singlet state to the nearby excited triplet state.[16] The benefit of choosing WLC instead of tuning the central wavelength of a conventional fs laser pulse lies in that the former naturally circumvents the tedious search for the energy position where the ISC process attains the largest probability (or the best efficiency). Secondly, once the excited triplet state is thus populated, a situation of population inversion could be naturally created in the triplet space because of the occurrence of non-populated lower triplet state(s), most likely resulting in photon emission. This may open the possibility of tracking in real time the pure triplet dynamics through monitoring the transient change of such photon emission via time-resolved optical spectroscopy.

In an attempt to examine the validity of the above hypotheses, we resort to the routinely used fs pump–WLC probe technique[17] but adopt an unconventional scheme. Conventionally, a preceding

pump laser is applied to excite the molecular sample and a subsequent WLC probe laser follows the ensuing response. As the probing light is fed into a spectrometer that can barely withstand high-power irradiation, the probe power is usually much lower than the pump power. Still within the weak probing regime, we take a time-reversed version of the conventional pump–probe scheme (termed fs-TRPP for short), where the weak WLC "probe" precedes, rather than follows, the strong "pump". This is somewhat similar to the so-called perturbed field induction decay technique that has been employed to detect the vibrational relaxation within molecular ground state.[18,19] Notably, in the present case the emission change as a consequence of the population modulation effect exerted by the delayed "pump", rather than the pump-induced probe absorption (or transmission) change, is detected.

Since the conventional pump–probe scheme is also employed in this study for comparison, the terminology of "pump" and "probe" (by convention) is *nominally* retained for the fs-TRPP case. To avoid any unwanted confusions, we stress here that in the TRPP regime the delayed "pump" actually acts as a population modulator instead of the regular excitation source, whereas the preceding WLC "probe" plays a dual role as the real optical excitation source and also the carrier of the "pump"-modulated emission (ME) signals that will be subjected to differential detection (i.e., with the modulating "pump" laser being chopped on and off alternately).

We here report, by performing a set of such fs-TRPP experiments on a proof-of-concept molecular system [i.e., the malachite green (MG) molecule], that the pure triplet dynamics can be singled out and further mapped out through monitoring the transient ME signals that are proven to arise solely from the dark triplet space. With the assistance of crude (yet rational) modeling and simulations, we have been able to capture some interesting details of the pure triplet dynamics to a certain extent.

Methods

Femtosecond pump–probe experiments. The fs pump–probe experiments (in both conventional and TRPP regimes) were performed on a modified ExciPro system (CDP) in combination with a 25-fs amplified laser system (Coherent). The schematic of the optical layout is depicted in Fig. 1, in which the definition of delay-time sign is specifically indicated (with the unusual fs-TRPP regime being highlighted). The experimental details can be found in Supplementary Information.†

Steady-state absorption and fluorescence spectroscopy. The steady-state absorption (230–1320 nm) and fluorescence (560–800 nm) spectra were recorded, under ambient conditions, on a SolidSpec-3700DUV UV-Vis-NIR Spectrophotometer (Shimadzu) and an FLS920 fluorescence spectrometer (Edinburgh), respectively. Both the MG and Rhodamine 6G (R6G) samples were prepared in aqueous solution with an identical concentration of 3.6 μM. The fluorescence spectra were obtained under excitation at the iso-absorptive wavelength of 552 nm.

First-principles calculations. Molecular models were built for the MG molecule. The optimized geometry, electronic structures, and vibronic profiles (normal modes) were simulated with the density function theory (DFT) using the Gaussian 09 package at the B3LYP/6-31++G** level.[20] The water solvent effect was considered with the polarizable continuum model. The time-dependent DFT calculations at the same level[21] were conducted to find out the excited states (for both singlets and triplets) and to generate the single-photon absorption spectrum. The linear coupling model was used to compute the Franck–Condon distributions with the program we developed in 2005.[22] More computational details regarding the distribution profiles of the absorption and ultrafast spectra as well as the considerations of environmental effect are given in Supplementary Information.†

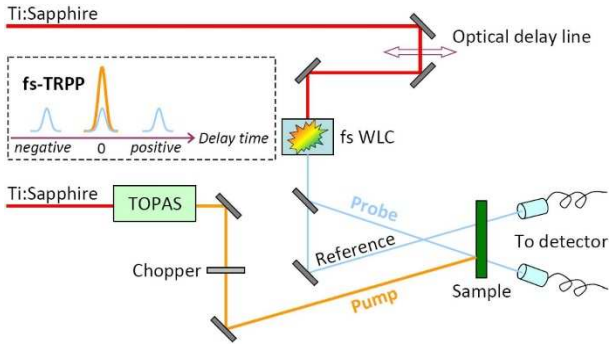

Fig. 1 Schematic optical layout of the fs pump–probe experiments. The inset (dashed box) defines the delay-time signs by convention.

Results and discussion

1 The choice of molecule for proof of concept: Aspect of fluorescing behavior

MG ($C_{23}H_{25}ClN_2$; molecular structure in the inset of Fig. 2) was proven a good prototypical molecule to materialize our proposed concept as its fluorescence-inert nature[23] can simplify the situation by eliminating as much interference as possible from the singlet-space fluorescence. A distinctive comparison between MG and R6G in terms of fluorescing ability is shown in Fig. 2, from which the fluorescence quantum yield of MG is estimated to be more than three orders of magnitude lower than that of R6G (excitation at the iso-absorptive wavelength of 552 nm). Further considerations regarding MG's fluorescing behavior are discussed later, in conjunction with the analysis on the assignment of our time-resolved pump–probe data.

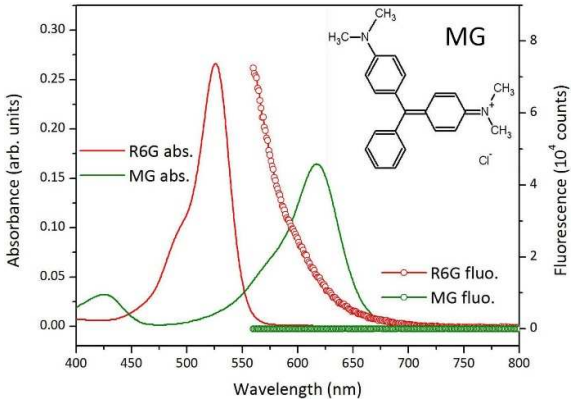

Fig. 2 Steady-state absorption and fluorescence spectra of the MG molecule of interest and the R6G molecule as a reference. Both samples were prepared in aqueous solution with an identical concentration of 3.6 μM. The inset shows the molecular structure of MG.

2 The choice of molecule for proof of concept: Aspect of state energetics

Most relevantly, our first-principles calculations on MG (involving two water molecules and one electron) revealed that the high-lying singlet and triplet states of MG are fairly close in energy. For instance, the S_2 and T_3 states are nearly degenerate (see the shaded region in Fig. 3), which implies a high efficiency of ISC ($S_2 \rightarrow T_3$). Schematically partitioned into two spaces (simply for clarity) in Fig. 4 are the singlets (S_1 and S_2) and triplets (T_1, T_2, and T_3) of relevance to this study, which are depicted with reference to the observed (for singlets) and computed (for triplets) energetics as seen from Fig. 3.

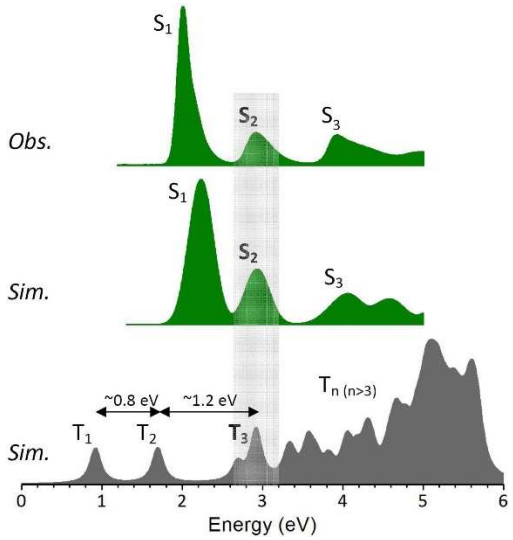

Fig. 3 Energetics of the electronically excited states reflected in the steady-state absorption spectra of MG. *Obs*., observed; *Sim*., simulated; S, singlet; T, triplet.

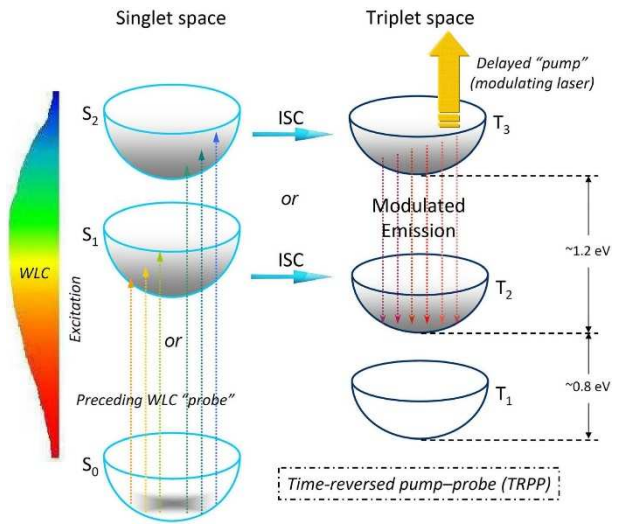

Fig. 4 Schematic illustration of how to map out the pure triplet dynamics in the MG molecule by means of fs-TRPP.

3 The observation of modulated emission solely from the triplet space

The two-dimensional map in Fig. 5a exhibits the fs-TRPP transients recorded on an aqueous MG sample (1.5 mM), in the form of differential transmission of the WLC "probe", $\Delta T/T_0 = (T - T_0)/T_0$, where T (T_0) denotes the "probe" transmission in the presence (absence) of the "pump" whose central wavelength is 580 nm (pulse duration ~60 fs, spectral width ~20 nm). Note that, based on the analysis below, this transient pattern is determined to originate solely from the ME carried by the WLC "probe", as *nominally* presented in terms of $\Delta T/T_0$. This typical set of data spectrally covers an energy region of 1.2–1.8 eV (689–1033 nm) provided by the chirp-corrected WLC "probe" and temporally ranges from 0 to –3 ps (in negative delay times) with 50-fs scanning steps. Markedly, the absolute amplitudes of these transients are comparable to those of the regular transmission signals recorded via conventional pump–probe (see Supplementary Fig. S1).†

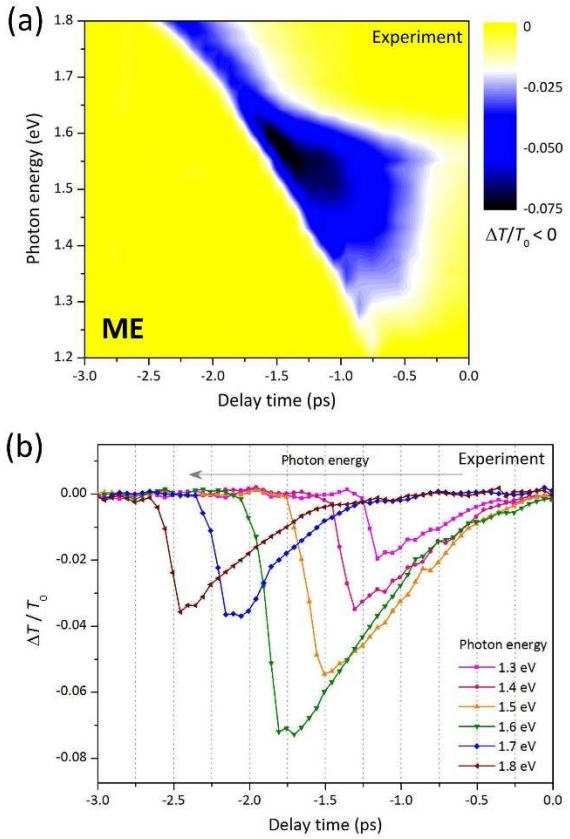

Fig. 5 Pure triplet dynamics mapped out in the MG molecule via ME. (a) The "pump"-modulated, negatively valued ME ($T_3 \rightarrow T_2$) transients observed in the fs-TRPP measurements on an aqueous MG sample (1.5 mM). (b) Representative kinetic traces taken at different probe photon energies (from 1.3 to 1.8 eV with 0.1-eV steps).

It should be emphasized here that our very cautious check with the WLC's chirp compensation (using the ExiPro 2.6 software), the determination of delay time zero (by cross-correlating the pump and probe pulses at the sample cell in situ), and the WLC's pre-pulsing (see also the experimental details in Supplementary Information)† has safely excluded the possibility that such fs-TRPP transients are associated with any related artifacts.

Displayed in Fig. 5b are several representative kinetic traces taken at different "probe" photon energies (extracted from Fig.

5a), from which two distinctive features can be seen. Firstly, they all exponentially "grow" (in terms of the absolute amplitude) with the delay times being swept from zero towards negative direction (down to –3 ps), but then reach maximum at certain delay times, and right afterwards recover very rapidly. The apparent time constants for the initial build-up at different photon energies are on the same timescale (330–620 fs), so are those for the subsequent recovery (~100 fs). The relevant kinetics fitting results are collected in Supplementary Fig. S2.† Secondly, the delay times at which the signals reach maximum, t_{max} (on the picosecond timescale), are well separated for different photon energies in a the-higher-the-later manner (~250-fs lag for each 0.1-eV increment).

4 The feature and assignment of the triplet emission transients

We find it unlikely that the observed fs-TRPP transients stand with the singlet space where the population build-up usually occurs on a much shorter timescale (likely within the instrument response function, ~100 fs). Rather, the observation of picosecond t_{max} could imply the population transfer from the singlet space to the triplet space (i.e., ISC). Reflecting the real-time population evolution of the triplet states under the naturally formed population-inversion condition as predicted before, these avalanche-like kinetics (Fig. 5b) manifest themselves as a relatively slow population built-up (till saturation at a certain threshold) followed by nearly instantaneous population depletion. In this particular case, it could be such sort of avalanche-like effect that renders the emission signals strong enough to be comparable, in terms of the absolute amplitude, to the regular singlet-space differential transmission signals (refer to Supplementary Fig. S1).† At this stage the exact physical origin of the observed avalanche-like kinetics is still unknown. We feel that it is related to the shape of the potential energy surface of the triplet states that can somewhat significantly reduce the nonradiative decay between the triplet states. Another possibility is that since the relationship between the phases of each frequency component in the WLC pulse could be very complicated, such complication may be implicated in the observed avalanche-like kinetics. In the fs-TRPP regime, the wavepackages launched by the WLC pulses could be quite different from those by "quasi-monochromatic" fs pulses, and such difference may correlate to the enhancement of ISC probability via the broadband WLC excitation.

The photoexcitation drives a manifold of molecules into an excited state; however, each molecule only hosts one exciton. In other words, the broadband WLC can excite different molecules differently. In the present case, the preceding WLC launches transitions of either $S_0 \rightarrow S_1$ or $S_0 \rightarrow S_2$ (not both). Then, the observed fs-TRPP transients can, in principle, be attributed to two possible emission channels: either $T_3 \rightarrow T_2$ (or T_1) [via ISC ($S_2 \rightarrow T_3$)] or $T_2 \rightarrow T_1$ [via ISC ($S_1 \rightarrow T_2$)]. We assign the scythe-shaped pattern (blue-to-black region in Fig. 5a) as stemming from ME between different vibrational level pairs of T_3 and T_2 [hereafter denoted ME ($T_3 \rightarrow T_2$) for clarity] that falls in an energy region just above 1.2 eV by noting $\Delta E(T_3–T_2) \approx 1.2$ eV (see Figs. 3 and 4). This assignment is supported by a set of control experiments described as follows.

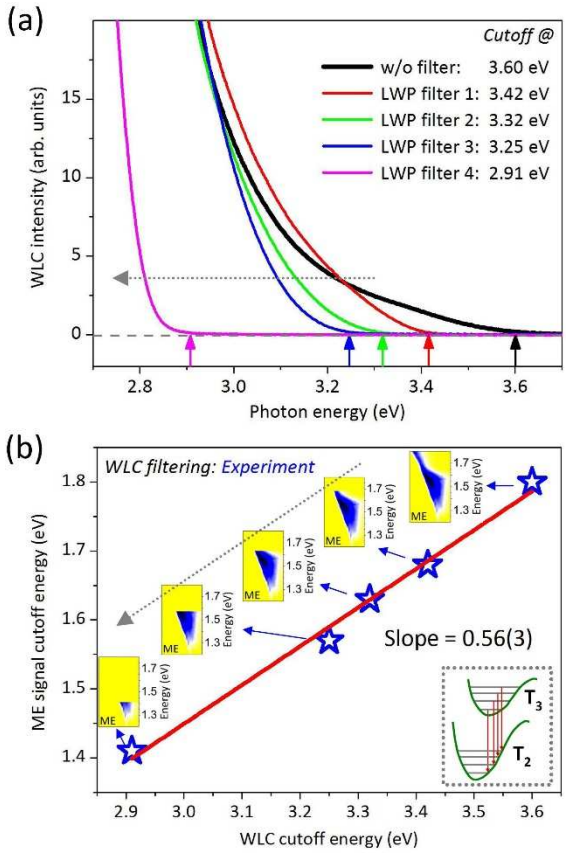

Fig. 6 (a) The use of the four LWP filters (colored lines) to chop the high-frequency components of the original, broad WLC spectrum (thick, black line) makes the high-photon-energy portions of the observed ME transients (shown in Fig. 5a) systematically disappear, as exhibited in (b). (b) The WLC filtering results show a clear linear dependence of the ME cutoff energies (insets in chains) vs. the corresponding WLC cutoff energies [marked in (a)], which implies a potential shift between T_3 and T_2 caused by Franck–Condon distributions (schematically depicted in the lower-corner inset).

5 The control experiments to verify the assignment of triplet emission transients

When the high-frequency components of the broad WLC spectrum (0.8–3.6 eV; see Supplementary Fig. S3)† were systematically chopped by using several long-wave-pass filters (Fig. 6a), the high-photon-energy portions of the pattern disappeared correspondingly (Fig. 6b). This is understandable because the high-frequency filtering simply shifts downward the highest-lying, populated vibrational manifolds of the S_2 state in a controlled manner, and so does those of the nearby T_3 state given the ISC's iso-energetic nature.[11] Further, when the WLC spectrum was chopped by using the filters with cutoffs below 2.7 eV, the entire pattern vanished (see Supplementary Fig. S3).† Under these circumstances the S_2 manifolds (onset at ~2.7 eV; refer to Fig. 3) are no longer subjected to the WLC's excitation and consequently the T_3 manifolds will not be populated at all, thus diminishing any $T_3 \rightarrow T_2$ emissions. Interestingly, plotting the ME ($T_3 \rightarrow T_2$) cutoff energies vs. the corresponding WLC cutoff energies yields a clear linear dependence (Fig. 6b), which implies a potential shift between T_3 and T_2 caused by Franck–Condon distributions.[24] It should be pointed out here that we have

employed several different centre wavelengths for the "pump" (such as 480, 530, and 640 nm), all of which turned out to generate essentially the same transient pattern as the representative one (580 nm) reported here (Fig. 5a). This conforms well to the fact that triplet states lying above T_3 (labeled $T_{n(n>3)}$ in Fig. 3) abound, thus making the modulating "pump" laser readily find a way out for resonantly driving vibronic transitions from T_3 to these higher-lying triplet states. Such insensitivity to the "pump" wavelengths in the fs-TRPP regime validates its role as a population modulator.

It can be safely inferred from the above WLC filtering tests that the probability of ISC ($S_2 \rightarrow T_3$) should be much higher than that of ISC ($S_1 \rightarrow T_2$); if otherwise, we would have also observed the alternative ME ($T_2 \rightarrow T_1$) channel that falls in an energy region roughly above 0.8 eV by noting $\Delta E(T_2–T_1) \approx 0.8$ eV (refer to Figs. 3 and 4), which is however not the case. In fact, the lower probability of ISC ($S_1 \rightarrow T_2$) is compatible with the relatively large (~0.4 eV) energy mismatch between S_1 and T_2.

6 Ruling out the possible interference from MG's fluorescence

For the MG molecule, the fluorescence from S_1 to S_0 is rather weak[23] while that from S_2 to S_0 is relatively more intense,[25] it is thus important to take caution with any possibilities that MG's fluorescence may interfere with what we observed in the fs-TRPP measurements.

On the one hand, the $S_1 \rightarrow S_0$ fluorescence can be safely ruled out to account for the observed emission (1.2–1.8 eV; Fig. 5a), because the energy separation between S_1 and S_0 exceeds 1.8 eV (see the experimental steady-state absorption spectrum shown in Fig. 3), as also confirmed by our conventional pump–probe measurements (580-nm laser excites the S_1 state followed by a WLC probing; see Supplementary Fig. S1)[†] where the observed transient features associated with the transitions of $S_0 \rightarrow S_1$ (ground-state bleach) and $S_1 \rightarrow S_0$ (stimulated emission) are all in the energy region that exceeds 1.8 eV.

On the other hand, let us examine the other two possible fluorescing processes in the singlet space: $S_2 \rightarrow S_0$ and $S_2 \rightarrow S_1$. In fact, the $S_2 \rightarrow S_0$ fluorescence can be readily ruled out because of the quite large (>2.5 eV according to the steady-state absorption spectrum in Fig. 3) energy separation between S_2 and S_0. Admittedly, the $S_2 \rightarrow S_1$ fluorescence, if any, may interfere with what we observed in the triplet space, as the energy separation between S_2 and S_1 is likely within 1.2–1.8 eV according to the steady-state absorption spectrum (Fig. 3). However, in this particular system of MG molecule, the transition between S_2 and S_1 is not favored, as confirmed by our conventional pump–probe measurements (580-nm laser excites the S_1 state followed by a WLC probing; see Supplementary Fig. S1)[†] where only the excited-state absorption (ESA) transients assigned to the $S_1 \rightarrow S_3$ transition (around 2 eV) were observed while no ESA transients associated with the $S_1 \rightarrow S_2$ transition were observed in the energy region of 1.2–1.8 eV (i.e., the specific energy region for our observed $T_3 \rightarrow T_2$ emission; see Fig. 5a).

7 An auxiliary pump–probe study using conventional scheme

In addition to the above fs-TRPP results, we have also performed measurements using the conventional pump–probe scheme, where the singlet-space stimulated emission transients were readily identified using a preceding 580-nm pump and a delayed WLC probe (refer to Supplementary Fig. S1).[†] It is natural to ask if any similar stimulated emission transients in the triplet space (termed SET for short) could also be discernable. In the present case, the "quasi-monochromatic" (as compared to the much broader bandwidth of WLC) 580-nm pump drives the vibronic transitions of $S_0 \rightarrow S_1$, as schematically depicted in Fig. 7. Besides, the energy mismatch between S_1 and T_2 is relatively large (~0.4 eV; refer to Figs. 3 and 4). These two factors are obviously not in favor of the ISC ($S_1 \rightarrow T_2$) pathway. We nevertheless anticipate that they might compromise, to a large extent, with the much higher power afforded by the strong pump, producing a sufficient amount of MG molecules in their T_2 state. This may open the possibility of using a delayed WLC probe to directly track the SET ($T_2 \rightarrow T_1$) dynamics, which presumably occurs in the near infrared spectral region by noting $\Delta E(T_2–T_1) \approx 0.8$ eV.

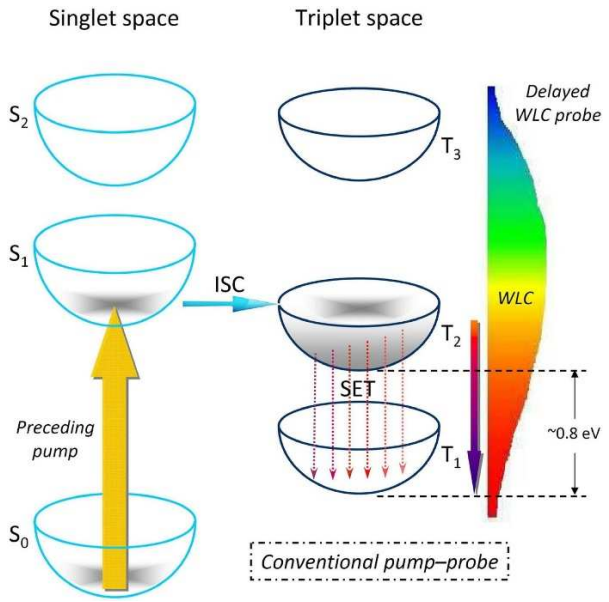

Fig. 7 Schematic illustration of SET as an auxiliary tool for tracking the population dynamics in the triplet space.

Indeed, we did observe the SET transients within 0.8–1.2 eV, as shown in Fig. 8a. Given the energy region it is safe to ascribe the observed pattern to the vibronic transitions of $T_2 \rightarrow T_1$. Several representative kinetic traces are displayed in Fig. 8b. The apparent relaxation time constants at different photon energies are ~500 fs on average.

It is worth noting that the energy-dependent t_{max} with SET ($T_2 \rightarrow T_1$), ~0.5–1.0 ps, turn out to be slightly shorter than those with ME ($T_3 \rightarrow T_2$). It is somewhat surprising to see that the population dynamics of both ME ($T_3 \rightarrow T_2$) and SET ($T_2 \rightarrow T_1$) violate Kasha's rule that generally governs photoluminescence in the singlet space,[11] suggesting relatively long lifetimes of the excited triplet states. Presumably, the aforementioned situation of population inversion naturally created in the triplet space may be related to such violation. Since both ME ($T_3 \rightarrow T_2$) and SET ($T_2 \rightarrow T_1$) stand with pure triplet states, this finding hints that applications demanding the breakdown of Kasha's rule[26,27] could

find an easier way out in the molecular triplet space.

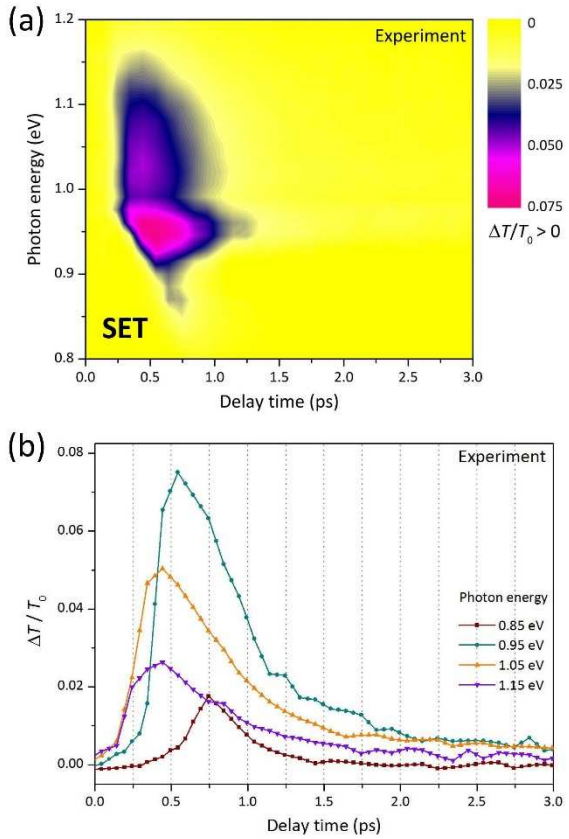

Fig. 8 Pure triplet dynamics mapped out in the MG molecule via SET. (a) The differential, positively valued SET ($T_2 \rightarrow T_1$) transients observed in the conventional pump–probe measurements on an aqueous MG sample (1.5 mM). (b) Representative kinetic traces observed at different probe photon energies (from 0.85 to 1.15 eV with 0.1-eV steps).

Last but not least, we have also performed another case study using a combination of WLC and 400-nm (instead of 580-nm) lasers. The relevant results and discussion are given in Supplementary Information (Fig. S4).† This comparative study provides collateral evidence supporting our above understanding on the ME and SET processes in this molecular system.

8 Insights from numerical simulations

To gain a better understanding of the transient population dynamics involved, we have attempted to develop a set of general rate equations taking account of various possible energy transfer/relaxation processes, especially the cascading processes of intramolecular vibrational redistribution (refer to Appendix to Supplementary Fig. S5),† which turns out to rationally accommodate the initial, exponential build-up behavior in the observed avalanche-like ME ($T_3 \rightarrow T_2$) kinetics. The reverse ISC ($T_3 \rightarrow S_2$) is also considered; as the T_3 manifolds are initially not populated, the ISC from S_2 to T_3 dominates, producing the observed ME ($T_3 \rightarrow T_2$). Particular attention has also been paid to the temporal evolution of the vibrational populations associated with the ME ($T_3 \rightarrow T_2$) as well as the SET ($T_2 \rightarrow T_1$); for instance, such evolution within both the T_3 manifolds (for ME) and the T_2 manifolds (for SET) has been reasonably simulated with a set of time constants of realistic physical meaning: 1.2, 10, and 0.05 ps for ISC, internal conversion, and intramolecular vibrational redistribution, respectively (see Supplementary Fig. S5).† It is noted that the internal conversion assumed here for the triplets is unusually slow, even slower than the ISC process. Admittedly, we have found that without such an assumption, it seems impossible to explain the avalanche-like emission observed in the experiments. Despite the necessary assumptions as well as the ignorance of such effects as thermalization[28] and conformational variation[29] in our crude modeling, these preliminary simulations may help us capture, to a certain extent, the essence of our experimental observations. Undoubtedly, a more accurate description from the theoretical perspective evokes a more rigorous yet sophisticated modeling framework that takes account of the currently neglected, intractable factors as much as possible.

Notably, our numerical simulations of the state energies and population dynamics just play a role of aid in the data interpretation rather than indispensable evidence. By noticing that we have nicely reproduced the singlet-state energies (see Fig. 3) using a molecular model that takes into account both hydrogen bonding and charge distribution due to ions interaction (see Supplementary Information),† we think it would be reasonable for us to use the simulated triplet-state energies as a good reference to our ultrafast dynamics study. As a matter of fact, there remains a lack of effective experimental means for one to look into the dark triplet space and further map out the real-time excited-state dynamics therein, thus one usually has to resort to the assistance from the theoretical calculations. This, to some extent, highlights the very contribution of our present study which introduces a new experimental configuration to this end.

Conclusions

We have introduced a strategy towards mapping of ultrafast excited-state dynamics in the molecular triplet space, which is established on the use of an unconventional femtosecond time-reversed pump–probe scheme to create temporal separation of the emission from the singlet space. Its validity and efficacy have been justified, to a satisfactory extent, by our proof-of-concept experiments on the prototypical molecule of malachite green. We envision that this technique may find its value in future applications in molecular luminescence/photonics and solar light harvesting that rely on effective manipulation between singlet and triplet spaces, to which the in-depth understanding of the excited-state dynamics in the dark triplet space would be beneficial.

Acknowledgements

This work was jointly supported by the MOST (2010CB923300 and 2014CB848900), the NSFC (21173205, 21121003, 91127042, 20925311, and 91221104), the CAS (XDB01020000), the FRFCU (WK2340000063), and the Recruitment Program of Global Experts in China.

Notes and references

[a] *Department of Chemical Physics, School of Chemistry and Materials Science, University of Science and Technology of China, Hefei, Anhui 230026, China. E-mail: qunzh@ustc.edu.cn*
[b] *Hefei National Laboratory for Physical Sciences at the Microscale, University of Science and Technology of China, Hefei, Anhui 230026, China. E-mail: jiangj1@ustc.edu.cn*
[c] *Synergetic Innovation Center of Quantum Information and Quantum Physics, University of Science and Technology of China, Hefei, Anhui 230026, China. E-mail: yiluo@ustc.edu.cn*
[d] *Department of Theoretical Chemistry, School of Biotechnology, Royal Institute of Technology, AlbaNova, S-106 91 Stockholm, Sweden.*

† Electronic Supplementary Information (ESI) available: Details of the femtosecond pump–probe experiments and the first-principles calculations, as well as a typical case study using conventional pump−probe scheme (Fig. S1), the ME ($T_3 \rightarrow T_2$) kinetics fitting results (Fig. S2), more details of WLC filtering tests (Fig. S3), another case study using a combination of WLC and 400-nm (instead of 580-nm) lasers and relevant discussions (Fig. S4), and the crude modeling/preliminary simulations on ME and SET (Fig. S5). See DOI: 10.1039/xxxxxxxx/

1 M. C. DeRosa and R. J. Crutchley, *Coord. Chem. Rev.*, 2002, **233–234**, 351–371.
2 C. Schweitzer and R. Schmidt, *Chem. Rev.*, 2003, **103**, 1685–1757.
3 A. Endo, K. Sato, K. Yoshimura, T. Kai, A. Kawada, H. Miyazaki and C. Adachi, *Appl. Phys. Lett.*, 2011, **98**, 083302.
4 K. Goushi, K. Yoshida, K. Sato and C. Adachi, *Nature Photon.*, 2012, **6**, 253–258.
5 H. Uoyama, K. Goushi, K. Shizu, H. Nomura and C. Adachi, *Nature*, 2012, **492**, 234–238.
6 K. Sato, K. Shizu, K. Yoshimura, A. Kawada, H. Miyazaki and C. Adachi, *Phys. Rev. Lett.*, 2013, **110,** 247401.
7 Y. Shao and Y. Yang, *Adv. Mater.*, 2005, **17**, 2841–2844.
8 C.-M. Yang, C.-H. Wu, H.-H. Liao, K.-Y. Lai, H.-P. Cheng, S.-F. Horng, H.-F. Meng and J.-T. Shy, *Appl. Phys. Lett.*, 2007, **90,** 133509.
9 R. Srinivasan, J. S. Feenstra, S. T. Park, S. Xu and A. H. Zewail, *Science*, 2005, **307,** 558–563.
10 M. Kasha, *Disc. Faraday Soc.*, 1950, **9**, 14–19.
11 J. R. Lakowicz, *Principles of Fluorescence Spectroscopy*, Springer, New York, 2006.
12 P. Hannaford, *Femtosecond Laser Spectroscopy*, Springer, New York, 2005.
13 E. E. Ostroumov, R. M. Mulvaney, R. J. Cogdell and G. D. Scholes, *Science*, 2013, **340,** 52–56.
14 D. S. N. Parker, R. S. Minns, T. J. Penfold, G. A. Worth and H. H. Fielding, *Chem. Phys. Lett.*, 2009, **469**, 43–47.
15 R. S. Minns, D. S. N. Parker, T. J. Penfold, G. A. Worth and H. H. Fielding, *Phys. Chem. Chem. Phys.*, 2010, **12**, 15607–15615.
16 H. Yersin, *Top. Curr. Chem.*, 2004, **241**, 1–26.
17 R. Berera, R. van Grondelle and J. T. M. Kennis, *Photosynth. Res.*, 2009, **101,** 105–118.
18 K. Wynne and R. M. Hochstrasser, *Chem. Phys.*, 1995, **193,** 211–236.
19 P. Hamm, *Chem. Phys.*, 1995, **200,** 415–429.
20 M. J. Frisch, G. W. Trucks, H. B. Schlegel, G. E. Scuseria, M. A. Robb, J. R. Cheeseman, G. Scalmani, V. Barone, B. Mennucci, G. A. Petersson, H. Nakatsuji, M. Caricato, X. Li, H. P. Hratchian, A. F. Izmaylov, J. Bloino, G. Zheng, J. L. Sonnenberg, M. Hada, M. Ehara, K. Toyota, R. Fukuda, J. Hasegawa, M. Ishida, T. Nakajima, Y. Honda, O. Kitao, H. Nakai, T. Vreven, J. A. Montgomery, Jr., J. E. Peralta, F. Ogliaro, M. Bearpark, J. J. Heyd, E. Brothers, K. N. Kudin, V. N. Staroverov, R. Kobayashi, J. Normand, K. Raghavachari, A. Rendell, J. C. Burant, S. S. Iyengar, J. Tomasi, M. Cossi, N. Rega, J. M. Millam, M. Klene, J. E. Knox, J. B. Cross, V. Bakken, C. Adamo, J. Jaramillo, R. Gomperts, R. E. Stratmann, O. Yazyev, A. J. Austin, R. Cammi, C. Pomelli, J. W. Ochterski, R. L. Martin, K. Morokuma, V. G. Zakrzewski, G. A. Voth, P. Salvador, J. J. Dannenberg, S. Dapprich, A. D. Daniels, Ö. Farkas, J. B. Foresman, J. V. Ortiz, J. Cioslowski and D. J. Fox, *Gaussian 09 Revision A.1*, Gaussian Inc., Wallingford CT, 2009.
21 M. Caricato, B. Mennucci, J. Tomasi, F. Ingrosso, R. Cammi, S. Corni and G. Scalmani, *J. Chem. Phys.*, 2006, **124**, 124520.
22 Y. H. Wang, M. Halik, C. K. Wang, S. R. Marder and Y. Luo, *J. Chem. Phys.*, 2005, **123**, 194311.
23 J. R. Babendure, S. R. Adams and R. Y. Tsien, *J. Am. Chem. Soc.*, 2003, **125**, 14716–14717.
24 M. Lax, *J. Chem. Phys.*, 1952, **20,** 1752–1760.
25 M. Yoshizawa, K. Suzuki, A. Kubo and S. Saikan, *Chem. Phys. Lett.*, 1998, **290**, 43–48.
26 P. Klan and J. Wirz, *Photochemistry of organic compounds*, Wiley, Chichester, 2009.
27 C. L. Choi, H. Li, A. C. K. Olson, P. K. Jain, S. Sivasankar and A. P. Alivisatos, *Nano Lett.*, 2011, **11**, 2358–2362.
28 A. J. Taylor, D. J. Erskine and C. L. Tang, *Chem. Phys. Lett.*, 1984, **103**, 430–435.
29 A. Mokhtari, L. Fini and J. Chesnoy, *J. Chem. Phys.*, 1987, **87**, 3429–3435.